Autonomous Robots 13, 207–222, 2002

Dynamic Motion Planning for Mobile Robots Using Potential Field Method

S.S. GE AND Y.J. CUI
Department of Electrical Engineering, National University of Singapore, Singapore 117576, Singapore
elegesz@nus.edu.sg

Abstract. The potential field method is widely used for autonomous mobile robot path planning due to its elegant mathematical analysis and simplicity. However, most researches have been focused on solving the motion planning problem in a stationary environment where both targets and obstacles are stationary. This paper proposes a new potential field method for motion planning of mobile robots in a dynamic environment where the target and the obstacles are moving. Firstly, the new potential function and the corresponding virtual force are defined. Then, the problem of local minima is discussed. Finally, extensive computer simulations and hardware experiments are carried out to demonstrate the effectiveness of the dynamic motion planning schemes based on the new potential field method.

Keywords: potential field, dynamic motion planning, mobile robots

1. Introduction

The potential field method is commonly used for autonomous mobile robot path planning in the past decade (Latombe, 1991; Borenstein and Koren, 1989, 1991; Chuang and Ahuja, 1998; Rimon and Koditschek, 1992; Khatib, 1986; Rimon, 1990; Kim and Khosla, 1992; Ko and Lee, 1996; Hussien, 1989; Khosla and Volpe, 1988; Veelaert and Bogaerts, 1999; Warren, 1989, 1990; Canny and Lin, 1990). The basic concept of the potential field method is to fill the robot's workspace with an artificial potential field in which the robot is attracted to its target position and is repulsed away from the obstacles (Latombe, 1991). This method is particularly attractive because of its elegant mathematical analysis and simplicity. Most of the previous studies use potential field methods to deal with mobile robot path planning in stationary environments where targets and obstacles were all stationary. However, in many real-life implementations, the environments are dynamic. Not only the obstacles are moving, so does the target.

In an effort to solve the problem of motion planning in a dynamic environment where the obstacles are moving, one approach is to include time as one of the dimensions of the model world and thus the moving obstacles can be regarded as stationary in the extended world (Fujimura and Samet, 1989; Shih and Lee, 1990; Conn and Kam, 1998). Accordingly, the dynamic motion planning problem is reduced to motion planning in stationary environments. The major problem in this approach is that it always assume that the trajectories of the moving obstacles are known a priori, which are often inapplicable in real applications.

Another approach was proposed in Ko and Lee (1996) and Hussien (1989) which extended the potential field method to the problems of moving obstacle avoidance by constructing repulsive potential functions which take into account the velocity information. In Ko and Lee (1996), though the velocity of the obstacle is considered when building the repulsive potential, the velocity of the robot is not taken into account. This is inadequate because the possibility of the collision between the robot and obstacle depends on the relative position and velocity between them. The repulsive potential function in Hussien (1989) makes fully use of the velocity information of the robot and the obstacle. However, it was assumed that the relative velocity of the robot with respect to the obstacle is invariant irregardless of the position of the robot and its partial derivatives in terms of position is zero. This assumption is unrealistic as the relative

velocity is actually a function of the position of the robot and its derivatives in terms of position cannot be considered as zero all the time. Both methods deal with obstacle avoidance problem with a stationary target.

In this paper, we propose a new potential field method for motion planning of a mobile robot in a dynamic environment where the target and obstacles are moving. The attractive potential is defined as a function of the relative position and velocity of the target with respect to the robot. By choosing different parameters, different performances, soft-landing and hard-landing problems, can be obtained. The repulsive potential is also defined as the relative position and velocity of the robot with respect to the obstacles. Accordingly, the virtual force is defined as the negative gradient of the potential in terms of both position and velocity rather than position only. The new definitions of the potential functions and the virtual forces allow the robot to track the target in a desired manner. Besides, this approach does not require that the trajectories of the obstacles are known a priori. Instead, the motion planning only needs the on-line measurements of the obstacles' information.

This paper is organized as follows: In Section 2, we give a brief description of the mobile robot motion planning problem in a dynamic environment. Section 3 presents the new attractive potential function and its properties. Section 4 gives a new definition of the repulsive potential function. Section 5 describes the local minimum problems. Computer simulation and hardware experiment studies are presented in Sections 6 and 7, respectively. Finally, a conclusion is given in Section 8.

2. Problem Statement

The motion planning problem of a mobile robot in a dynamic environment is to plan and control the robot motion from an initial position to track a moving target in a desired manner while avoiding moving obstacles. The robot can either soft-land on the target where the velocity of the robot is the same as that of the target at landing, or hard-land on the target when there is no requirement on the velocity of the robot when the robot reaches the target. To simplify the analysis, we make the following assumptions:

Assumption 1. The shape, position $\mathbf{p}$ and velocity $\mathbf{v}$ of the robot are known.

Assumption 2. The position $\mathbf{p}_{tar}$ and velocity $\mathbf{v}_{tar}$ of the target are known with $|\mathbf{v}_{tar}| < v_{\max}$.

Assumption 3. The obstacles are convex polygons whose shapes, positions $\mathbf{p}_{obsi}$ and velocities $\mathbf{v}_{obsi}$, $i = 1, 2, \ldots, n_{obs}$, where n_{obs} is the number of obstacles, can be accurately measured on-line.

3. Attractive Potential Function

Conventionally, the attractive potential is defined as a function of the relative distance between the robot and the target only where the target is a fixed point in space. In our research, it was found that it is beneficial to have the velocities of the robot and the target considered in the construction of the potential field. Additional degrees of freedom are being introduced for different tracking performances. When the target is moving, the conventional pure position based potential function is not directly applicable and has to be modified. In this paper, the potential field functions are presented as follows

$$U_{att}(\mathbf{p}, \mathbf{v}) = \alpha_p \|\mathbf{p}_{tar}(t) - \mathbf{p}(t)\|^m + \alpha_v \|\mathbf{v}_{tar}(t) - \mathbf{v}(t)\|^n \tag{1}$$

where $\mathbf{p}(t)$ and $\mathbf{p}_{tar}(t)$ denote the positions of the robot and the target at time t, respectively; $\mathbf{p} = [x\ y\ z]^T$ in a 3-dimensional space or $\mathbf{p} = [x\ y]^T$ in a 2-dimensional space; $\mathbf{v}(t)$ and $\mathbf{v}_{tar}(t)$ denote the velocities of the robot and the target at time t, respectively; $\|\mathbf{p}_{tar}(t) - \mathbf{p}(t)\|$ is the Euclidean distance between the robot and the target at time t; $\|\mathbf{v}_{tar}(t) - \mathbf{v}(t)\|$ is the magnitude of the relative velocity between the target and the robot at time t; α_p and α_v are scalar positive parameters; and m and n are positive constants.

From (1), the attractive potential $U_{att}(\mathbf{p}, \mathbf{v})$ approaches its minimum zero if and only if the relative distance and velocity between the robot and the target are zero. The attractive potential $U_{att}(\mathbf{p}, \mathbf{v})$ increases as the relative distance and/or velocity between the robot and the target increase.

It is easy to see that if $\alpha_v = 0$ and $m = 2$, the new attractive potential function (1) degenerates to the conventional quadratic form

$$U_{att}(\mathbf{p}, \mathbf{v}) = U_{att}(\mathbf{p}) = \alpha_p \|\mathbf{p}_{tar}(t) - \mathbf{p}(t)\|^2 \tag{2}$$

which does not contain the velocity information of the robot or the target. The corresponding conventional

virtual attractive force is defined as the negative gradient of the attractive potential in terms of position

$$\mathbf{F}_{att}(\mathbf{p}) = -\nabla U_{att}(\mathbf{p}) = -\frac{\partial U_{att}(\mathbf{p})}{\partial \mathbf{p}} \tag{3}$$

The new attractive potential $U_{att}(\mathbf{p}, \mathbf{v})$ is a function of both the position $\mathbf{p}$ and velocity $\mathbf{v}$ of the robot. Therefore, we shall define the corresponding virtual attractive force as the negative gradient of the attractive potential in terms of both position and velocity, i.e.

$$\begin{aligned}\mathbf{F}_{att}(\mathbf{p}, \mathbf{v}) &= -\nabla U_{att}(\mathbf{p}, \mathbf{v}) \\ &= -\nabla_p U_{att}(\mathbf{p}, \mathbf{v}) - \nabla_v U_{att}(\mathbf{p}, \mathbf{v})\end{aligned} \tag{4}$$

where

$$\nabla_p U_{att}(\mathbf{p}, \mathbf{v}) = \frac{\partial U_{att}(\mathbf{p}, \mathbf{v})}{\partial \mathbf{p}} \tag{5}$$

$$\nabla_v U_{att}(\mathbf{p}, \mathbf{v}) = \frac{\partial U_{att}(\mathbf{p}, \mathbf{v})}{\partial \mathbf{v}} \tag{6}$$

with the subscripts p and v denoting the gradient in terms of position and velocity, respectively.

With regards to the selection of m and n, we have the following remark to make.

Remark 1. Note that $U_{att}(\mathbf{p}, \mathbf{v})$ is not differentiable with respect to $\mathbf{p}$ at $\mathbf{p} = \mathbf{p}_{tar}$ for $0 < m \leq 1$, and with respect to $\mathbf{v}$ at $\mathbf{v} = \mathbf{v}_{tar}$ for $0 < n \leq 1$, respectively. The choice of m and n may cause a problem for certain applications but certainly not for all applications. Applications can be roughly divided into soft-landing and hard-landing problems. By soft-landing, we mean that the robot touches the moving target at zero relative velocity and then travels at the same velocity as the target. Hard-landing refers to those applications when the mission is regarded as completed when $\mathbf{p} = \mathbf{p}_{tar}$, irregardless of the magnitude of velocity.

When $\mathbf{p} \neq \mathbf{p}_{tar}$ and $\mathbf{v} \neq \mathbf{v}_{tar}$, substituting (1) into (4), we have

$$\mathbf{F}_{att}(\mathbf{p}, \mathbf{v}) = \mathbf{F}_{att1}(\mathbf{p}) + \mathbf{F}_{att2}(\mathbf{v}) \tag{7}$$

where

$$\mathbf{F}_{att1}(\mathbf{p}) = m\alpha_p \|\mathbf{p}_{tar}(t) - \mathbf{p}(t)\|^{m-1} \mathbf{n}_{RT} \tag{8}$$

$$\mathbf{F}_{att2}(\mathbf{v}) = n\alpha_v \|\mathbf{v}_{tar}(t) - \mathbf{v}(t)\|^{n-1} \mathbf{n}_{VRT} \tag{9}$$

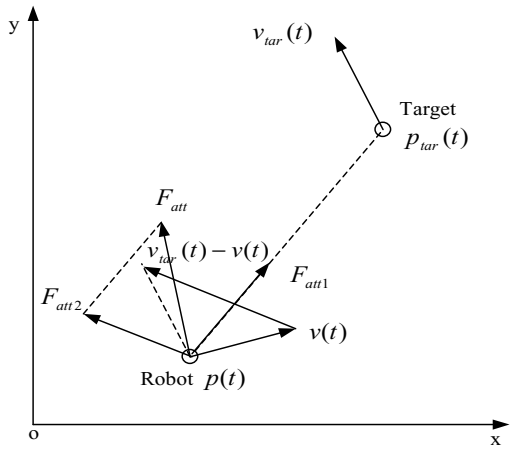

Figure 1. New attractive force in 2D space.

with $\mathbf{n}_{RT}$ being the unit vector pointing from the robot to the target and $\mathbf{n}_{VRT}$ being the unit vector denoting the relative velocity direction of the target with respect to the robot. The relationship between the attractive force and the position and velocity of the robot and the target in a 2-dimensional space is illustrated in Fig. 1. The attractive force $\mathbf{F}_{att}$ consists of two components: while the first component, $\mathbf{F}_{att1}(\mathbf{p})$, pull the robot to the target and shortens the distance between them, the second component, $\mathbf{F}_{att2}(\mathbf{v})$, "tries" to drive the robot to move at the same velocity of the target.

From Eqs. (8) and (9), for $m > 1$ and $n > 1$, when the robot approaches the target, i.e. $\|\mathbf{p}_{tar}(t) - \mathbf{p}(t)\|$ approaches zero, $\mathbf{F}_{att1}$ approaches zero; when the velocity of the robot approaches that of the target, $\mathbf{F}_{att2}$ approaches zero. Thus, when both the position and velocity of the robot approach those of the target, the attractive force $\mathbf{F}_{att}$ approaches zero, i.e. when the robot catches the target and travels at the same velocity of the target, the attractive force is zero and thus the robot moves together with the target. Such choices of m and n are necessary for solving soft-landing problems. In hard-landing problems, however, there is no such a constraint to m and n as long as $m, n > 0$.

4. Repulsive Potential Function

To solve moving obstacle avoidance, an intuitive way is to take into account the relative positions and velocities between the robot and the obstacles when constructing the repulsive potential function. In this section, a new repulsive potential function is presented which makes

fully use of the position and velocity information of the obstacles.

For simplicity of analysis and understanding, let us first take arbitrary convex obstacles and a point robot as an example to illustrate the construction of the new repulsive potential function, which can be easily modified in actual applications by taking into account the actual shape and size of the robot. Assume that the position $\mathbf{p}_{obs}(t)$ and velocity $\mathbf{v}_{obs}(t)$ of the nearest point on the obstacle to the robot can be obtained on-line. The relative velocity between the robot and the obstacle in the direction from the robot to the obstacle is given by

$$v_{RO}(t) = [\mathbf{v}(t) - \mathbf{v}_{obs}(t)]^T \mathbf{n}_{RO} \tag{10}$$

where $\mathbf{n}_{RO}$ is a unit vector pointing from the robot to the obstacle. If $v_{RO}(t) \leq 0$, i.e. the robot is moving away from the obstacle, no avoidance motion is needed. If $v_{RO}(t) > 0$, i.e. the robot is moving close to the obstacle, avoidance motion needs to be implemented.

Assume that at time t, the robot is moving toward the obstacle. The shortest distance between the robot and the body of the obstacle is denoted by $\rho_s(\mathbf{p}(t), \mathbf{p}_{obs}(t))$. Consider the case where the robot moves toward the obstacle, i.e. $v_{RO}(t) > 0$. If a maximum deceleration of magnitude $a_{\max}$ is applied to the robot to reduce its velocity, the distance traveled by the robot before v_{RO} reduces to zero is

$$\rho_m(v_{RO}) = \frac{v_{RO}^2(t)}{2a_{\max}} \tag{11}$$

Accordingly, the repulsive potential can be defined as follows

$$U_{rep}(\mathbf{p}, \mathbf{v}) = \begin{cases} 0, & \text{if } \rho_s(\mathbf{p}, \mathbf{p}_{obs}) - \rho_m(v_{RO}) \geq \rho_0 \text{ or } v_{RO} \leq 0 \\ \eta\left(\dfrac{1}{\rho_s(\mathbf{p}, \mathbf{p}_{obs}) - \rho_m(v_{RO})} - \dfrac{1}{\rho_0}\right), & \\ \quad \text{if } 0 < \rho_s(\mathbf{p}, \mathbf{p}_{obs}) - \rho_m(v_{RO}) < \rho_0 & \\ \quad \text{and } v_{RO} > 0 & \\ \text{not defined,} & \\ \quad \text{if } v_{RO} > 0 \text{ and } \rho_s(\mathbf{p}, \mathbf{p}_{obs}) < \rho_m(v_{RO}) & \end{cases} \tag{12}$$

where U_{rep} denotes the repulsive potential generated by the obstacle; ρ_0 is a positive constant describing the influence range of the obstacle; and η is a positive constant.

Note that when $\rho_s(\mathbf{p}, \mathbf{p}_{obs}) < \rho_m(v_{RO})$, the repulsive potential is not defined, since there is no possible solution to avoid collision with the obstacle in the aforementioned case where the robot moves toward the robot. From (12), we can see that when the robot is far away from the obstacle, i.e. $\rho_s(\mathbf{p}, \mathbf{p}_{obs}) - \rho_m(v_{RO}) \geq \rho_0$, the robot is not influenced by the obstacle, and therefore no avoidance motion is implemented. When the robot is within the influence range of the obstacle and $\rho_s(\mathbf{p}, \mathbf{p}_{obs})$ approaches $\rho_m(v_{RO})$, the repulsive potential approaches infinity and as the projection of relative velocity of the robot v_{RO} increases, the repulsive potential also increases. Even if the distance between the robot and the obstacle does not approach zero, the repulsive potential approaches infinity if the relative velocity v_{RO} is large enough.

Similar to the definition of the new attractive force, the corresponding new repulsive force is defined as the negative gradient of the repulsive potential in terms of both position and velocity

$$\begin{aligned} \mathbf{F}_{rep}(\mathbf{p}, \mathbf{v}) &= -\nabla U_{rep}(\mathbf{p}, \mathbf{v}) \\ &= -\nabla_p U_{rep}(\mathbf{p}, \mathbf{v}) - \nabla_v U_{rep}(\mathbf{p}, \mathbf{v}) \end{aligned} \tag{13}$$

The relative velocity of the robot with respect to the obstacle in the direction from the robot to the obstacle, $v_{RO}(t)$, can be written as

$$\begin{aligned} v_{RO}(t) &= (\mathbf{v}(t) - \mathbf{v}_{obs}(t))^T \mathbf{n}_{RO} \\ &= (\mathbf{v}(t) - \mathbf{v}_{obs}(t))^T (\mathbf{p}_{obs}(t) - \mathbf{p}(t))/ \\ &\quad \|\mathbf{p}_{obs}(t) - \mathbf{p}(t)\| \end{aligned} \tag{14}$$

The gradients of $v_{RO}(t)$ with respect to both velocity and position are given respectively as

$$\begin{aligned} \nabla_v v_{RO}(t) &= \mathbf{n}_{RO} \\ \nabla_p v_{RO}(t) &= \frac{1}{\|\mathbf{p}(t) - \mathbf{p}_{obs}(t)\|} \\ &\quad \times [v_{RO}(t)\mathbf{n}_{RO} - (\mathbf{v}(t) - \mathbf{v}_{obs}(t))] \end{aligned} \tag{15}$$

where $v_{RO}(t)\mathbf{n}_{RO}$ gives the velocity component of $\mathbf{v}(t) - \mathbf{v}_{obs}(t)$ in the direction from the robot to the obstacle.

For clarity, let $v_{RO\perp}(t)\mathbf{n}_{RO\perp}$ denote the velocity component perpendicular to $v_{RO}(t)\mathbf{n}_{RO}$ as given in the following equation

$$v_{RO\perp}\mathbf{n}_{RO\perp} = \mathbf{v}(t) - \mathbf{v}_{obs}(t) - v_{RO}(t)\mathbf{n}_{RO} \tag{16}$$

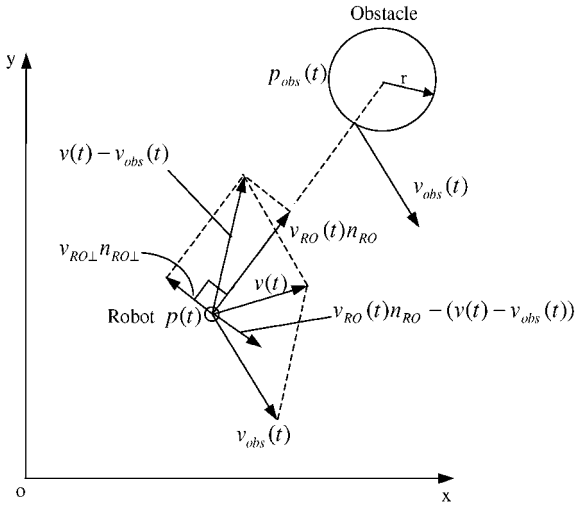

Figure 2. Vectors for defining the new repulsive potential.

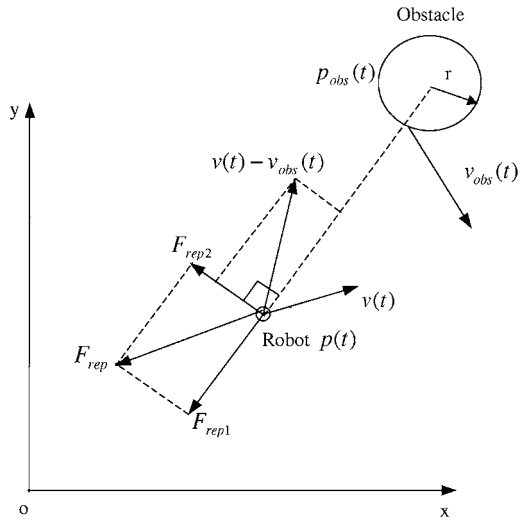

Figure 3. New repulsive force in 2D space.

where

$$v_{RO\perp} = \sqrt{\|\mathbf{v}(t) - \mathbf{v}_{obs}(t)\|^2 - v_{RO}(t)^2}$$
$$\mathbf{n}_{RO\perp}^T \mathbf{n}_{RO} = 1$$

Therefore, Eq. (15) can be simply expressed as

$$\nabla_p v_{RO}(t) = -\frac{1}{\|\mathbf{p}(t) - \mathbf{p}_{obs}(t)\|} v_{RO\perp} \mathbf{n}_{RO\perp} \quad (17)$$

Figure 2 shows the detailed relationships among the vectors.

The virtual repulsive force generated by the obstacle is then given by

$$\mathbf{F}_{rep}(\mathbf{p}, \mathbf{v}) = \begin{cases} 0, & \text{if } \rho_s(\mathbf{p}, \mathbf{p}_{obs}) - \rho_m(v_{RO}) \geq \rho_0 \text{ or } v_{RO} \leq 0 \\ \mathbf{F}_{rep1} + \mathbf{F}_{rep2}, & \\ & \text{if } 0 < \rho_s(\mathbf{p}, \mathbf{p}_{obs}) - \rho_m(v_{RO}) < \rho_0 \\ & \qquad \text{and } v_{RO} > 0 \\ \text{not defined}, & \\ & \text{if } v_{RO} > 0 \text{ and } \rho_s(\mathbf{p}, \mathbf{p}_{obs}) < \rho_m(v_{RO}) \end{cases} \quad (18)$$

where

$$\mathbf{F}_{rep1} = \frac{-\eta}{(\rho_s(\mathbf{p}, \mathbf{p}_{obs}) - \rho_m(v_{RO}))^2} \left(1 + \frac{v_{RO}}{a_{\max}}\right) \mathbf{n}_{RO} \quad (19)$$

and

$$\mathbf{F}_{rep2} = \frac{\eta v_{RO} v_{RO\perp}}{\rho_s(\mathbf{p}, \mathbf{p}_{obs}) a_{\max} (\rho_s(\mathbf{p}, \mathbf{p}_{obs}) - \rho_m(v_{RO}))^2} \mathbf{n}_{RO\perp} \quad (20)$$

The relationship between the repulsive force components in a 2D space is shown in Fig. 3. The repulsive force component $\mathbf{F}_{rep1}$ is in the opposite direction of $v_{RO}\mathbf{n}_{RO}$ which will keep the robot away from the obstacle. The repulsive force component $\mathbf{F}_{rep2}$ is in the same direction of $v_{RO\perp}\mathbf{n}_{RO\perp}$, and will act as a steering force for detouring.

In practical applications, the physical size of the robot has to be taken into consideration when constructing the repulsive potentials. For clarity of demonstration, let us consider a cylindrical robot of radius ρ_{rob}^*, and let $\rho_{rob} \geq \rho_{rob}^*$ be the radius of an artificial safety surface of the robot. The repulsive potential can be modified slightly as follows

$$U_{rep}(\mathbf{p}, \mathbf{v}) = \begin{cases} 0, & \\ & \text{if } \rho_s(\mathbf{p}, \mathbf{p}_{obs}) - \rho_{rob} - \rho_m(v_{RO}) \geq \rho_0 \text{ or } v_{RO} \leq 0 \\ \eta\left(\dfrac{1}{\rho_s(\mathbf{p}, \mathbf{p}_{obs}) - \rho_{rob} - \rho_m(v_{RO})} - \dfrac{1}{\rho_0}\right), & \\ & \text{if } 0 < \rho_s(\mathbf{p}, \mathbf{p}_{obs}) - \rho_{rob} - \rho_m(v_{RO}) < \rho_0 \\ & \qquad \text{and } v_{RO} > 0 \\ \text{not defined}, & \\ & \text{if } v_{RO} > 0 \text{ and } \rho_s(\mathbf{p}, \mathbf{p}_{obs}) - \rho_{rob} < \rho_m(v_{RO}) \end{cases}$$

Note that the introduction of ρ_{rob} is twofold. It not only defines the safety margin, $\rho_{rob} - \rho^*_{rob}$, of possible physical collision, but can also be used to accommodate any possible measurement uncertainty. One may choose a large ρ_{rob} for cases that (i) when the uncertainty of the range measurements is large, say when sonar sensors are used, and/or (ii) one wants a high safety margin of physical collision. On the other hand, a smaller ρ_{rob} is desirable for cases (i) when range measurements are accurate (say when a laser range finder is used), and (ii) small impact collision is allowed.

After the calculation of the attractive and repulsive forces, the total virtual force can be obtained by

$$\mathbf{F}_{total} = \mathbf{F}_{att} + \mathbf{F}_{rep} \tag{21}$$

where $\mathbf{F}_{att}$ and $\mathbf{F}_{rep}$ can be calculated through Eqs. (7) and (18). For the case where there are multiple obstacles, the repulsive force is given by

$$\mathbf{F}_{rep} = \sum_{i=1}^{n_{obs}} \mathbf{F}_{repi} \tag{22}$$

where n_{obs} is the number of obstacles and $\mathbf{F}_{repi}$ is the repulsive force generated by the ith obstacle. The total virtual force $\mathbf{F}_{total}$ will be used for motion planning.

5. Problems of Local Minima

When employing the new potential functions for dynamic motion planning, local minimum problems do exist and should be taken care of. For example, consider the case when the robot, the obstacle and the target move in the same direction along the same line and the obstacle is in between, as shown in Fig. 4. Assuming that the target moves outward or synchronously with the obstacle (this assumption ensures that the obstacle is between the robot and the target all the time), the robot is obstructed by the obstacle and cannot reach the target.

To solve the problem, the simplest method is to keep the robot moves according to the total virtual force as usual and wait for the obstacles or the target to change their motion. Since the environment is highly dynamic where both the target and the obstacles are moving, the situations where the configuration of the obstacles and target keeps static are rare. Thus, the waiting method is often adopted.

However, if after a certain period's waiting, the configuration of the obstacles and target is still unchanged and the robot is still trapped, it can then be assumed that the configuration will not change temporarily and the robot will have to take other approaches to escape from the trap situation. Since the configuration of the robot, obstacles and target is relatively stationary, the conventional local minimum recovery approaches such as wall following method, which were designed for the stationary environment cases, can be applied.

There is a special kind of local minimum problems which are generated because the target is within the influence range of the obstacle. For example, consider the case when the robot, the target and the obstacle lie on the same line with the target in the middle and both the target and the robot are close to the obstacle, as shown in Fig. 5. As the robot moves toward the target, it moves toward the obstacle as well. Due to the repulsive force generated by the obstacle, if the velocity of the robot is not large enough, the robot may not be able to reach the target though there is no obstacle between the robot and the target. This phenomenon is called free-path local minimum problem.

For example, consider a simple case where the target and the obstacle are stationary and lie on x-axis. Without loosing generality, we shall define the coordinate system fixed at the target with x-axis pointing to the obstacle which can be either stationary or moving. The relative position of the robot is denoted by x. For simplicity, let the mass of the robot be $m_{rob} = 1$ Kg and let the acceleration of the robot be determined by the Newton's Law. According to Eqs. (18), (21) and (7), the acceleration of the robot can be

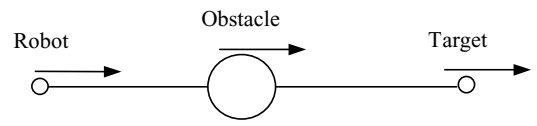

Figure 4. Local minimum problem.

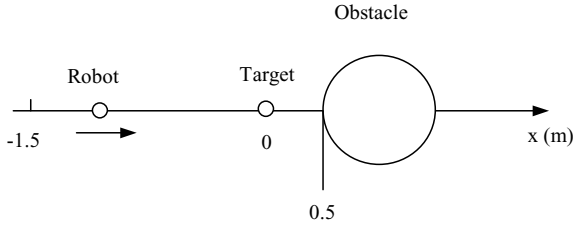

Figure 5. Free-path local minimum problem.

written as

$$\ddot{x} = -2\alpha_p x - 2\alpha_v \dot{x} - \eta^3 \left(\frac{1}{\rho_{TO} - x - \frac{\dot{x}^2}{2a_{\max}}} - \frac{1}{\rho_0} \right)^2 \times \left(1 + \frac{\dot{x}}{a_{\max}} \right) \quad (23)$$

where ρ_{TO} is the minimum distance between the target and the obstacle. Because it is difficult to obtain an analytic solution to the nonlinear Eq. (23), numerical analysis is used to investigate this differential equation. Figure 6 shows the numerical solutions for different initial velocities of the robot where the obstacle with radius $r = 0.3$ centers at $x = 0.8$ and the initial position of the robot is at $x = -1.5$. The parameters of the potential functions are set as $m = n = 2$, $\alpha_p = 0.005$, $\alpha_v = 0.1$, and $\eta = 0.2$. The influence range of the obstacle is 2 m. It is seen that (i) when the initial velocity of the robot is large enough, the robot can hard-land on the target, and (ii) when the initial velocity of the robot is small, the robot cannot reach the target though there is no obstacle between them.

To solve this problem, similar to the method in Ge and Cui (2000) which solves free-path local minimum problems in a stationary environment by modification of repulsive potential functions, the repulsive potential function herein may be modified to take into account the relative position and velocity between the robot and target. However, because the analysis for the dynamic case is difficult and complex, a decision making procedure is added to the motion planning system to solve the free-path local minimum problem conveniently: when the robot detects that both itself and the target are within the influence range of and obstacle, and the target is between the robot and the target, the parameter η is set to be zero, i.e. only the attractive force is taken into account. Thus, the robot can reach the target.

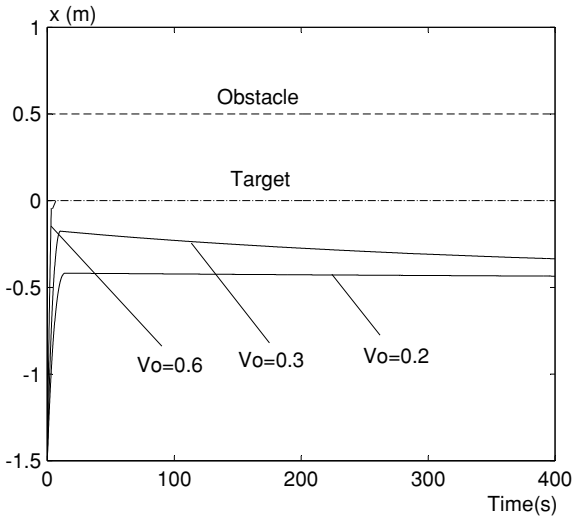

Figure 6. Path of robot with a free-path local minimum.

6. Motion Planning for Omnidirectional Mobile Robots

In potential fields methods, the total virtual force is used for motion planning. Different approaches have been proposed to use the total force to control the motion of the robots. For instance, the total force can be directly used as the control input or part of the control input to the low level controller of the robot (Rimon and Koditschek, 1992; Khatib, 1986; Guldner and Utkin, 1995; Kodtschek, 1989). The total force can also be used for only steering control such as in Borenstein and Koren (1989, 1991). In this paper, both motion planning strategies will be discussed. The selection of motion planning strategy depends on the type of the robot. The rest of this section will focuses on the discussion of motion planning for a holonomic omnidirectional mobile robot.

6.1. *Model of the Omnidirectional Robot*

Consider a holonomic omnidirectional mobile robot (Watanabe, 1998) which has full omnidirectionality with simultaneous and independently controlled rotational and translational motion capabilities. The mobile robot consists of three orthogonal wheels with the assembly mechanism proposed in Pin and Killough (1994).

Figure 7 shows the plane view of the robot, where $x - o - y$ and $x_b - o_b - y_b$ represent the global and body coordinate systems, respectively; θ denotes the orientation of the robot; D_1, D_2, and D_3 are the driving forces for the assemblies; and $\mathbf{F}_{rob}$ is the applied force which determines the translational motion of the robot by

$$m_{rob}\mathbf{a} = \mathbf{F}_{rob} \quad (24)$$

To convert the applied force $\mathbf{F}_{rob}$ into the driving input torque to individual wheel, the dynamic model of the robot needs to be considered. The driving system

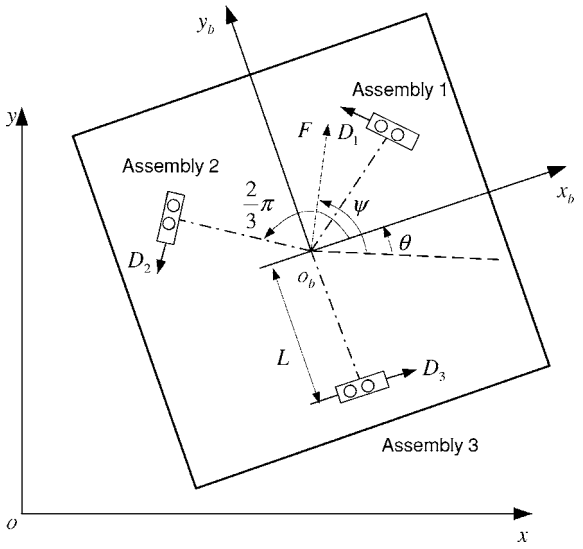

Figure 7. Model of the omnidirectional mobile robot.

for each assembly can be modeled by

$$I_w\dot{\omega}_i + c\omega_i = ku_i - rD_i \quad (i = 1, 2, 3) \tag{25}$$

where I_w is the moment of inertia of the wheel around the driving shaft; ω_i is the rotational rate of the wheel; c is the viscous friction factor for the wheel; r is the radius of the wheel; k is the driving gain factor; and u_i is the driving input torque. Define the state variable for the robot as $\mathbf{x} = [\dot{x}\ \ \dot{y}\ \ \dot{\theta}]^T$ and the manipulated variable as $\mathbf{u} = [u_1\ u_2\ u_3]^T$. Denote I_r as the moment of inertia of the robot and L as the distance between any assembly and the center of gravity of the robot, the dynamic model of the robot is given by Watanabe (1998)

$$\dot{\mathbf{x}} = A(\mathbf{x})\mathbf{x} + B(\mathbf{x})\mathbf{u} \tag{26}$$

where

$$A(\mathbf{x}) = \begin{bmatrix} \frac{-3c}{3I_w+2m_{rob}r^2} & \frac{-3I_w\dot{\theta}}{3I_w+2m_{rob}r^2} & 0 \\ \frac{3I_w\dot{\theta}}{3I_w+2m_{rob}r^2} & \frac{-3c}{3I_w+2m_{rob}r^2} & 0 \\ 0 & 0 & \frac{-3cL^2}{3I_wL^2+I_vr^2} \end{bmatrix}$$

$$B(\mathbf{x}) = \begin{bmatrix} \frac{-kr(\sqrt{3}\sin\theta-\cos\theta)}{3I_w+2m_{rob}r^2} & \frac{kr(\sqrt{3}\sin\theta-\cos\theta)}{3I_w+2m_{rob}r^2} & \frac{2kr\cos\theta}{3I_w+2m_{rob}r^2} \\ \frac{kr(-\sqrt{3}\cos\theta-\sin\theta)}{3I_w+2m_{rob}r^2} & \frac{kr(\sqrt{3}\cos\theta-\sin\theta)}{3I_w+2m_{rob}r^2} & \frac{2kr\sin\theta}{3I_w+2m_{rob}r^2} \\ \frac{krL}{3I_wL^2+I_vr^2} & \frac{krL}{3I_wL^2+I_vr^2} & \frac{krL}{3I_wL^2+I_vr^2} \end{bmatrix}$$

Apparently, the system is nonlinear and coupled. Nevertheless, using feedback linearization, we know that the control

$$\mathbf{u} = B(\mathbf{x})^{-1}(\mathbf{u}^* - A(\mathbf{x})\mathbf{x}) \tag{27}$$

can transform (26) into the following form

$$\dot{\mathbf{x}} = \mathbf{u}^* \tag{28}$$

where $\mathbf{u}^* = [\mathbf{a}^{*T}\ \ddot{\theta}^*]^T \in R^3$ is the new control signal to be determined, $\mathbf{a}^*$ is the desired acceleration of the robot, and θ^* is the desired orientation of the robot. For this holonomic omnidirectional robot, the orientation and the position can be controlled independently (Watanabe, 1998). In the following discussions, the orientation of the robot is assumed to be kept unchanged, i.e., $\ddot{\theta}^* = 0$.

6.2. *Motion Planning Strategy for Omnidirectional Robot*

From Eq. (28), it is easy to obtain that

$$\mathbf{a}^* = \mathbf{F}^*_{rob} \tag{29}$$

where $\mathbf{F}^*_{rob}$ is the desired force to be applied to the robot and can be obtained through the resultant total force.

The new attractive potential function contains four parameters, α_p, α_v, m, and n. By choosing different parameter settings, different performances can be obtained. Here, consider the case where $m = n = 2$ and assume that there is no obstacle in the workspace. From (8) and (9), the total force is given by

$$\mathbf{F}_{total} = 2\alpha_p(\mathbf{p}_{tar}(t) - \mathbf{p}(t)) + 2\alpha_v(\mathbf{v}_{tar}(t) - \mathbf{v}(t)) \tag{30}$$

Let the applied force to the robot be

$$\mathbf{F}^*_{rob} = m_{rob}\mathbf{a}_{tar} + \mathbf{F}_{total} \tag{31}$$

Combining with Eqs. (30) and (31), we have

$$\begin{aligned}\mathbf{a}^*(t) = \mathbf{a}_{tar}(t) &+ 2\alpha'_p(\mathbf{p}_{tar}(t) - \mathbf{p}(t)) \\ &+ 2\alpha'_v(\mathbf{v}_{tar}(t) - \mathbf{v}(t))\end{aligned} \tag{32}$$

where $\alpha'_p = \alpha_p/m_{rob}$ and $\alpha'_v = \alpha_v/m_{rob}$. Define $\mathbf{e}(t) = \mathbf{p}_{tar}(t) - \mathbf{p}(t)$ and Eq. (32) can be written as

$$\ddot{\mathbf{e}}(t) + 2\alpha'_v\dot{\mathbf{e}}(t) + 2\alpha'_p\mathbf{e}(t) = 0 \tag{33}$$

Because all the parameters in (33) are positive, system (33) is stable but with different performances for different choices of parameters. The characteristic equation is given by

$$s^2 + 2\xi\omega_n s + \omega_n^2 = 0 \tag{34}$$

where ξ and ω_n are the damping ratio and natural frequency of the system

$$\xi = \frac{\alpha_v'}{\sqrt{2\alpha_p'}} \tag{35}$$

$$\omega_n = \sqrt{2\alpha_p'} \tag{36}$$

For conventional attractive potential function, $\alpha_v = 0$, which leads to a zero damping ratio, the relative position between the robot and the target will oscillate with constant amplitude at the natural frequency ω_n, i.e. the robot will be oscillating around the target as will be verified by simulation later.

For the new attractive potential function, $\alpha_v > 0$, and the damping ratio $\xi > 0$. The position error reduces asymptotically. For $0 < \xi < 1$, the system is under damped—the tracking error converges to zero with oscillation. For $\xi > 1$, the system is over damped—there is no overshoot but the responses are very sluggish.

Remark 2. If there is no requirement of soft-landing, any positive α_p and α_v may be used to allow the robot to hit the target. However, if soft-landing is required, the velocity error should be zero once the robot reaches the target. When $\xi \geq 1$, the position and velocity of the robot approach those of the target as the time approaches infinity. That means the robot will soft-land on the target as time increases.

For other choices of m and n, different performances can be obtained. As the analytical analysis is difficult to obtain, numerical simulation investigations are presented next.

6.3. *Simulation Studies*

To show the effectiveness of the new motion planning scheme, extensive simulation studies are carried out for this omnidirectional mobile robot under realistic assumptions. In the simulation, it is assumed that the robot is of unit mass and its orientation does not change.

6.3.1. Moving Target Without Obstacles. When no obstacle exists in the space, the robot is influenced by the attractive potential only. In the following simulations, we shall investigate the performances of the new attractive potential function by assuming that there is no obstacle in the space. The target is moving from point $[10\ 10]^T$ at constant velocity, $\mathbf{v}_{tar} = [0.1\ -0.05]^T$. The initial position of the robot is $\mathbf{p}(0) = [1\ 1]^T$, its initial velocity is $[0\ 0]^T$.

For $m = n = 2$, firstly, we keep the parameter $\alpha_p = 0.005$ fixed and vary the parameter α_v to make the damping ratio of the system, $\xi = 0, 0.2, 1, 2$, which correspond to no damped, under damped, critical damped, and over damped systems, respectively. Figure 8 shows the paths of robot and target for all the cases. Clearly, the simulation results verify the analysis in Section 6.2. In practical implementations, for simplicity, m and n are usually chosen as $m = n = 2$, and for fast convergence of tracking errors with no oscillation, α_p and α_v are chosen such that the system has critical damping ratio. Figure 9 shows the simulation results for fixed $\xi = 1$ but with different parameters α_p and α_v. The larger the parameters α_p and α_v for fixed ξ, the faster the robot reaches the target. Therefore, for shorter time to reach the target, larger α_p and α_v are chosen.

For different performances, other choices of m, $n \neq 2$ can be chosen for the attractive potential function. Firstly, let us fix α_p, α_v and n and observe the different performances with different choices of m. Figure 10 shows the paths of the robot and the target in space for fixed $\alpha_p = 0.005$, $\alpha_v = 0.2$, $n = 2$, and

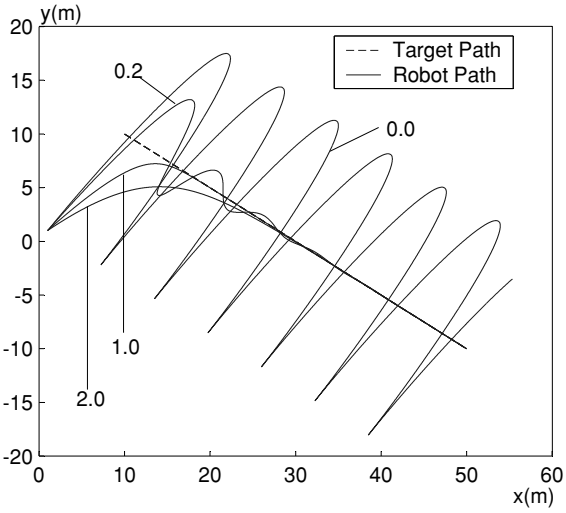

Figure 8. Paths of robot and target for different ξ with $m = n = 2$.

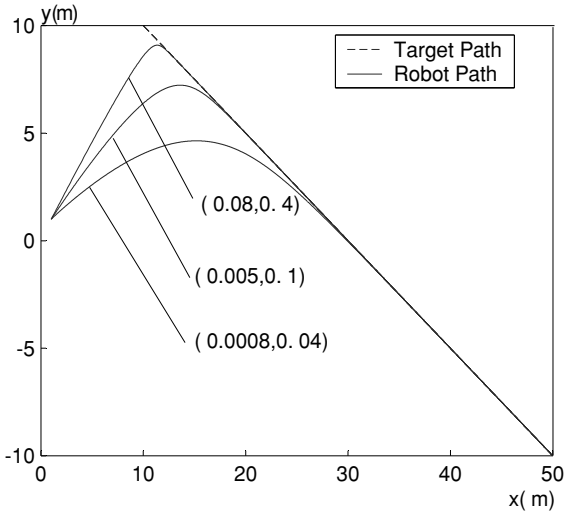

Figure 9. Paths of robot and target for different pairs of (α_p, α_v).

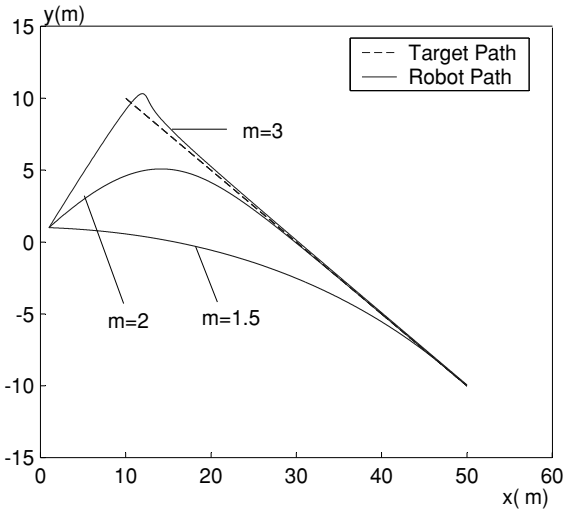

Figure 10. Paths of robot and target with no obstacles for $n = 2$.

different $m = 1.5$, 2, 3. It is shown that for fixed parameters α_p, α_v and n, the larger the parameter m, the faster the relative position between the robot and the target decrease.

Then, let us keep α_p and α_v unchanged and fix $m = 2$, and compare the performances for different choices of n. Figure 11 shows the paths of the robot and the target in these cases. It is shown that when parameters α_p, α_v and m are kept constant, the larger the parameter n, the quicker the position errors decreases. In the simulation, when $n = 3$, the position and velocity errors damp with oscillation.

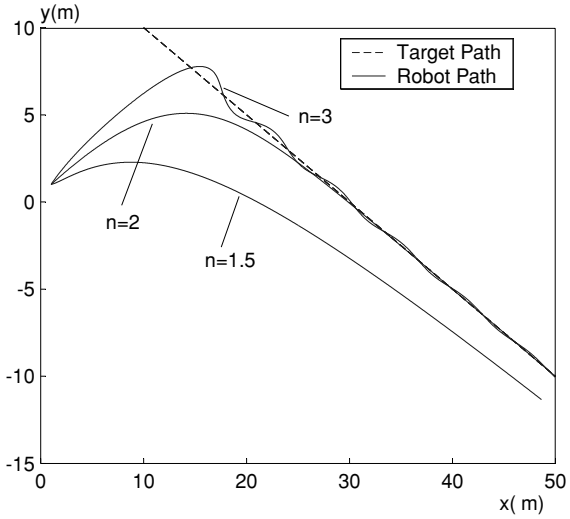

Figure 11. Paths of robot and target with no obstacles for $m = 2$.

For $0 < m \leq 1$ or $0 < n \leq 1$, from Eqs. (8) and (9), i.e.

$$\mathbf{F}_{att1}(\mathbf{p}) = m\alpha_p \|\mathbf{p}_{tar}(t) - \mathbf{p}(t)\|^{m-1}\mathbf{n}_{RT}$$
$$\mathbf{F}_{att2}(\mathbf{v}) = n\alpha_v \|\mathbf{v}_{tar}(t) - \mathbf{v}(t)\|^{n-1}\mathbf{n}_{VRT}$$

which are apparently not defined at $\mathbf{p} = \mathbf{p}_{tar}$ and at $\mathbf{v} = \mathbf{v}_{tar}$, respectively. These lead to discontinuous virtual attractive forces at these points which may cause abrupt changes of the acceleration of the robot. Therefore, $0 < m \leq 1$ or $0 < n \leq 1$ are not suitable for soft-landing problems. However, such choices can be used for hard-landing applications. Figure 12 shows the tracking performances for $m = 1$ and $n = 2$, where $\alpha_p = 0.05$ and $\alpha_v = 0.4$. Clearly, the robot can

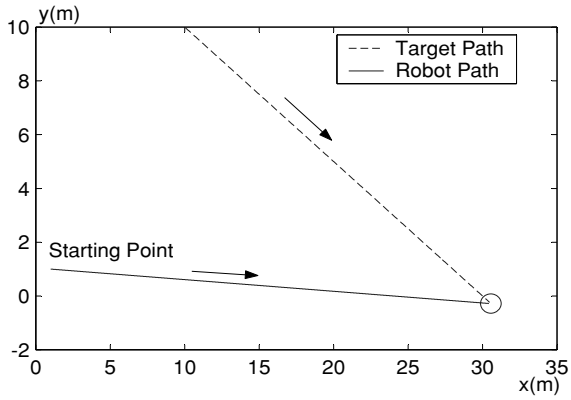

Figure 12. Path of robot and target for $m = 1$, $n = 2$.

successfully reach the target though the velocity of the robot is not equal to that of the target at landing.

6.3.2. Moving Target with Moving Obstacles. In practical applications, the ranges between the robot and obstacles are often measured by sensors on board and measurement noises are unavoidable. In order to make the simulations more realistic, uncertainties are added to the simulated measured ranges between the robot and obstacles. In the following simulations, the influence range of obstacles is set as $\rho_0 = 2$ m. The measurement noise is modeled by a white noise with zero mean and standard deviation 0.05 m, which represents an uncertainty of 2.5% and above of the true range value within the influence range of the obstacle.

Assume that the mobile robot moves in a dynamic environment where the target moves at constant velocity, $\mathbf{v}_{tar} = [0.1, -0.05]^T$ starting from point $[10, 10]^T$. Six obstacles exist in the environment, among which Obstacles 1, 2, and 3 are moving obstacles. Obstacle 1 moves at velocity $[0.0, 0.28]^T$ starting from point $[5, 0]^T$, Obstacle 2 moves at velocity $[-0.29, 0]^T$ from point $[9.4, 4.5]^T$, and Obstacle 3 moves at velocity $[-0.05, -0.065]^T$ from point $[19, 10]^T$. Obstacles 4, 5, and 6 are stationary obstacles located at $[8, 10.5]^T$, $[18, 4.5]^T$ and $[20, 7]^T$, respectively. The mobile robot starts moving from point $[1, 1]^T$ with zero initial velocity. The parameters of the attractive potential function are chosen as $m = n = 2, \alpha_p = 0.005$ and $\alpha_v = 0.1$; and the parameters of the repulsive potential function are chosen as $\eta = 0.3$ and $\rho_0 = 2$ m.

At first, the robot sets off from point $[1, 1]^T$ with zero initial velocity. It is far from the obstacles and is affected only by the target. At $t = 7$ s, the robot enters the influence range of Obstacle 1. As shown in Fig. 13, Obstacle 1 generates a repulsive force pointing upper left which makes the robot change its direction and try to detour Obstacle 1 from its front. As the robot moves on, it enters the influence ranges of Obstacle 2, which also generates a repulsive force pointing upper left. Now, both obstacles affect the robot simultaneously and accelerate the robot in the upper left direction. At $t = 13.6$ s, the robot moves away from the influence of Obstacle 1, thus the repulsive force generated by Obstacle 1, $\mathbf{F}_{rep1}$, is zero. From $t = 14.7$ s when the robot is in front of Obstacle 2 and moving upward, Obstacle 2 does not affect the robot any more and $\mathbf{F}_{rep2} = 0$. Then, the robot is again only affected by the target. As the robot turns right to follow the target, the robot moves toward Obstacle 1 again at time shot $t = 16.1$ s, then,

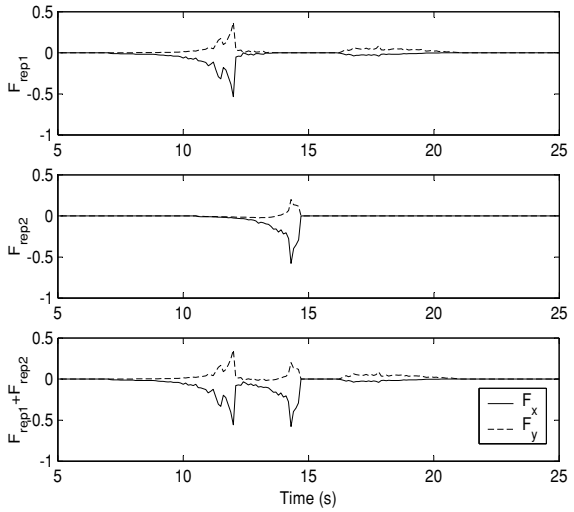

Figure 13. Repulsive forces generated by Obstacles 1 and 2.

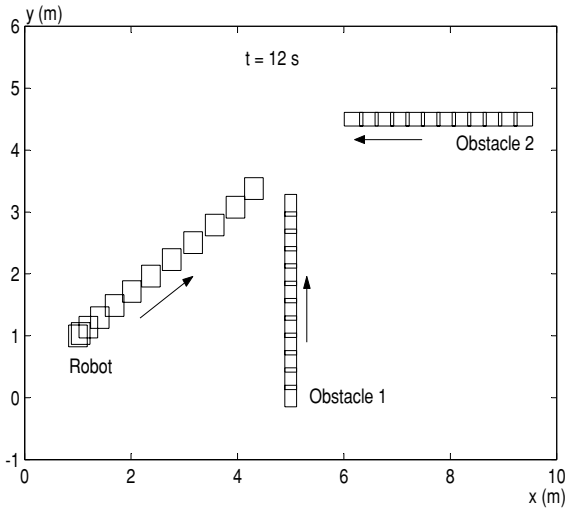

Figure 14. Paths of robot, Obstacles 1 and 2 at time $t = 12$ s.

$\mathbf{F}_{rep1}$ becomes nonzero again and also points upper left. The resultant force drives the robot to detour Obstacle 1 successfully at time shot $t = 21$ s. The paths of the robot and obstacles 1 and 2 at time shots $t = 12$ s, $t = 16$ s and $t = 22$ s are shown in Figs. 14–16 which clearly records how the robot avoids the two moving obstacles, and the repulsive forces generated by Obstacles 1 and 2 are shown in Fig. 13.

Then, the mobile robot moves according to the attractive force generated by the target till $t = 26.5$ s, when the robot enters the influence range of the stationary obstacle, Obstacle 4, which generates a repulsive force pointing the lower right direction, as

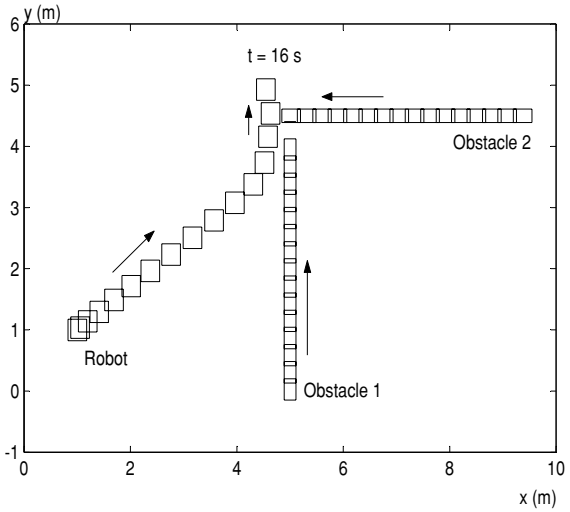

Figure 15. Paths of robot, Obstacles 1 and 2 at time $t = 16$ s.

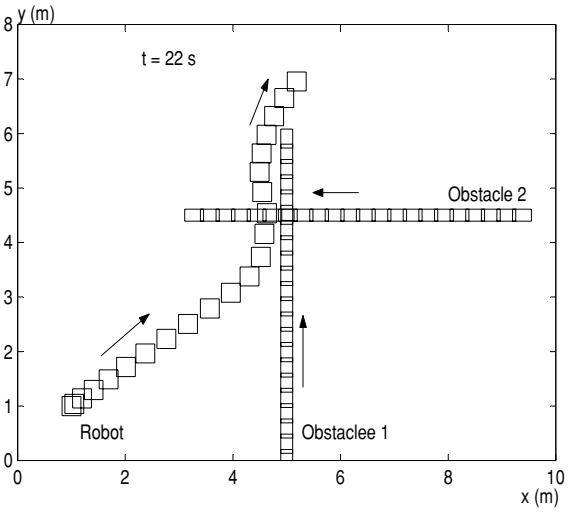

Figure 16. Paths of robot, Obstacles 1 and 2 at time $t = 22$ s.

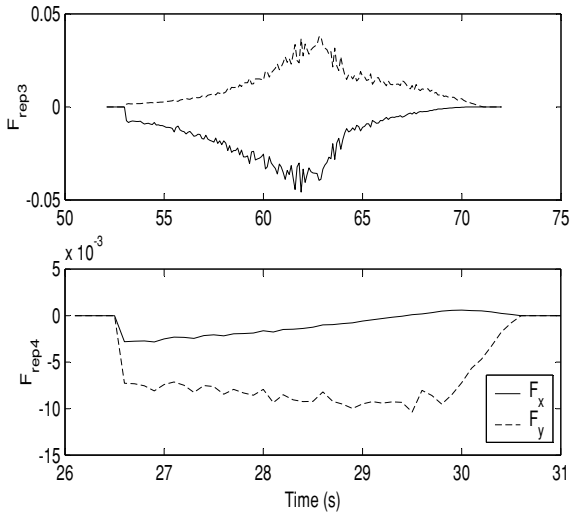

Figure 17. Repulsive forces generated by Obstacles 3 and 4.

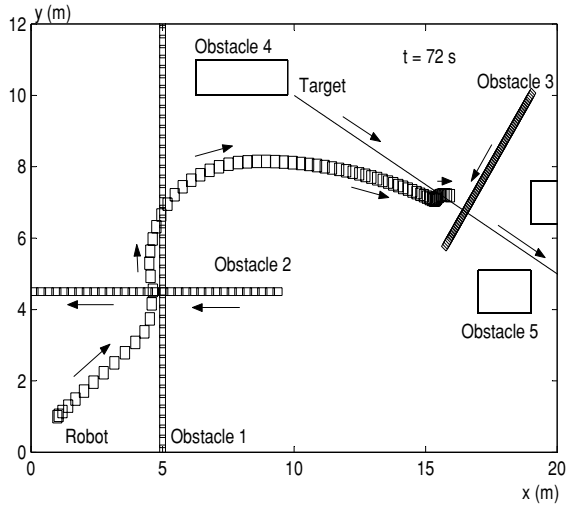

Figure 18. Paths of robot, target and Obstacles at $t = 72$ s.

shown in Fig. 17. At $t = 30.6$ s, the robot escapes from the influence range of Obstacle 4.

During the period of $t \in [30.6, 53.0]$s, the motion of the robot is determined only by the attractive force. After that, the robot enters the influence range of another moving obstacle, Obstacle 3. As shown in Fig. 17, it also generates a repulsive force in the upper left direction, which drives the robot to detour itself from behind. Figure 18 records the path of the robot, obstacles and target at time shot $t = 72$ s, from which it can be seen clearly how the robot detours Obstacle 3.

After the robot detoured Obstacle 3, it is affected by Obstacles 5 and 6 simultaneously. Together with the influence of the target, the total virtual force drives the robot to pass through between the two obstacles and finally soft land on the target at time shot $t = 212$. Figure 19 shows the compete paths of the robot, obstacles and target. It verifies that the robot can reach the target and avoid obstacles successfully.

7. Motion Planning for Differential Mobile Robot

The proposed potential field functions can be used for not only omnidirectional mobile robots, they can also be applied to other types of mobile robots. This section will describe the experimental results on a differential

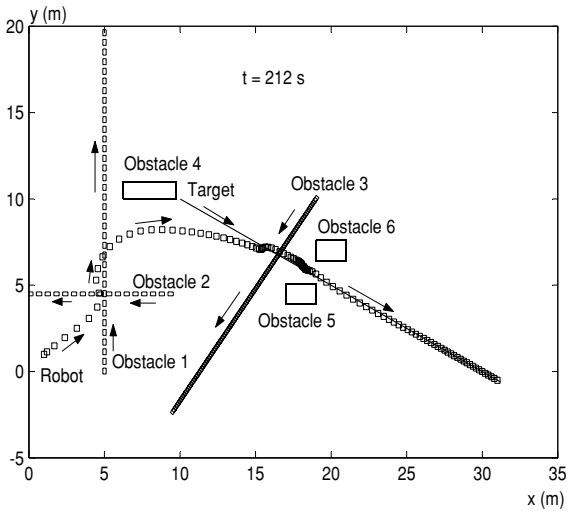

Figure 19. Paths of robot, target and obstacles.

drive mobile robot where the proposed potential field method is used for motion planning.

7.1. *Experimental Setup*

As shown in Fig. 20, the overall experimental system is actually a multi-robot system which consists of a host computer, a vision system, an RF communication system and several differential drive mobile robots. The robots, i.e., the YUJIN robots, were produced by the KAIST, Korea. Each robot has the same size (7.5 cm×7.5 cm×7.5 cm) and has two differential drive wheels. In the experimental studies, one of the robots serves as the mobile robot under investigation, and the others act as the target or obstacles. Each robot has its own driving mechanism, communication subsystem and CPU board. The communication subsystem receives the velocity command from the host computer and sends it to the CPU. The computational part controls the robot's velocity according to the command data through the driving mechanism. The video camera captures the images of the field where the robot moves and sends the signals to the host computer. All calculations on vision data processing and motion control of the robot are done in the host computer. From the vision data, the position and velocity of each robot can be calculated and are used for generating the motion control command. Then, the control commands are sent out through the RF transmitter to the mobile robots.

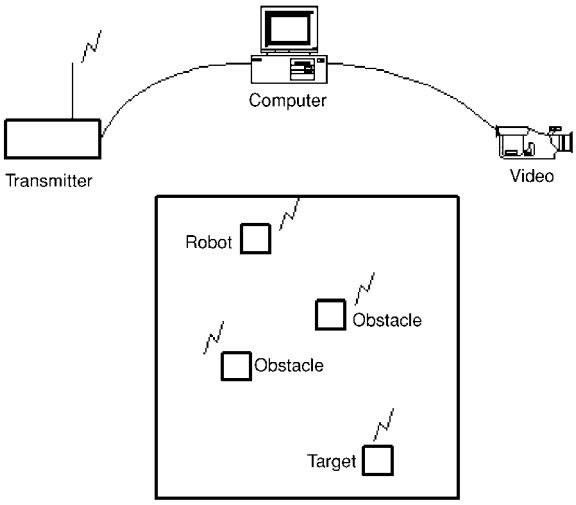

Figure 20. Experimental system.

7.2. *Model of Differential Drive Robot*

The top view of the YUJIN robot is shown in Fig. 21, where $x-o-y$ and $x_b-o_b-y_b$ denote the global and body coordinate systems, respectively; $L=7.5$ cm is the distance between the two wheels; v_l and v_r are the velocities of the left and right wheels; v is the velocity at the center of the robot; and θ is the orientation of the robot with respect to the global coordinate frame.

Denote the position of the robot as (x, y) and its turning rate as ω, then the kinematics equation of the robot is given by

$$\dot{x} = v\cos\theta \tag{37}$$

$$\dot{y} = v\sin\theta \tag{38}$$

$$\dot{\theta} = \omega \tag{39}$$

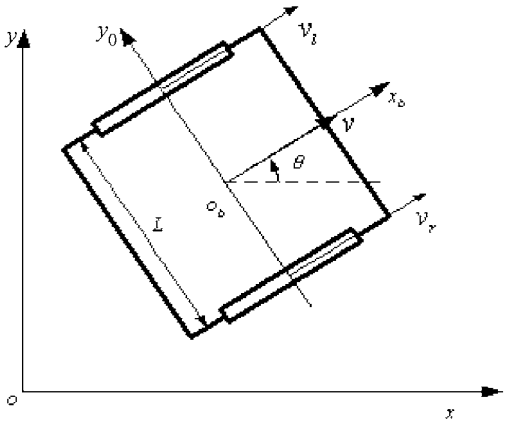

Figure 21. Model of the differential mobile robot.

For this robot, the real control input is the velocities of the left and right wheels, v_l and v_r, which have the following relationship with v and ω:

$$\begin{bmatrix} v_l \\ v_r \end{bmatrix} = \begin{bmatrix} 1 & \frac{L}{2} \\ 1 & -\frac{L}{2} \end{bmatrix} \begin{bmatrix} v \\ \omega \end{bmatrix} \tag{40}$$

7.3. Motion Planning Strategy

In the following experiments, the speed v of the robot is determined by the minimum distance between the robot and obstacles. When the robot is far from obstacles, its speed will be higher; and vice versa. Thus, the speed of the robot can be defined by

$$v = \begin{cases} v_{opt}, & \rho \geq \rho_0 \\ \frac{\rho}{\rho_0} v_{opt}, & \rho < \rho_0 \end{cases} \tag{41}$$

where v_{opt} is the maximum desired velocity of the robot when it is far from obstacles; ρ is the minimum distance between the robot and obstacles; and ρ_0 denotes the influence range of obstacles.

The resultant total force is used to control the turning rate ω of the mobile robot. Let θ_f be the angle of the total force $\mathbf{F}$, then the difference angle between θ_f and the orientation of the robot θ is given by

$$\theta_e = \theta_f - \theta \tag{42}$$

The steering rate of the robot is given by

$$\omega = K_s \theta_e \tag{43}$$

where K_s is a positive gain.

7.4. Experiment Results

In the experiment, the robot was expected to catch the moving target robot and simultaneously avoid some moving or stationary obstacles. The experimental result is shown in Fig. 22 with nine photos, (a)–(i), taken

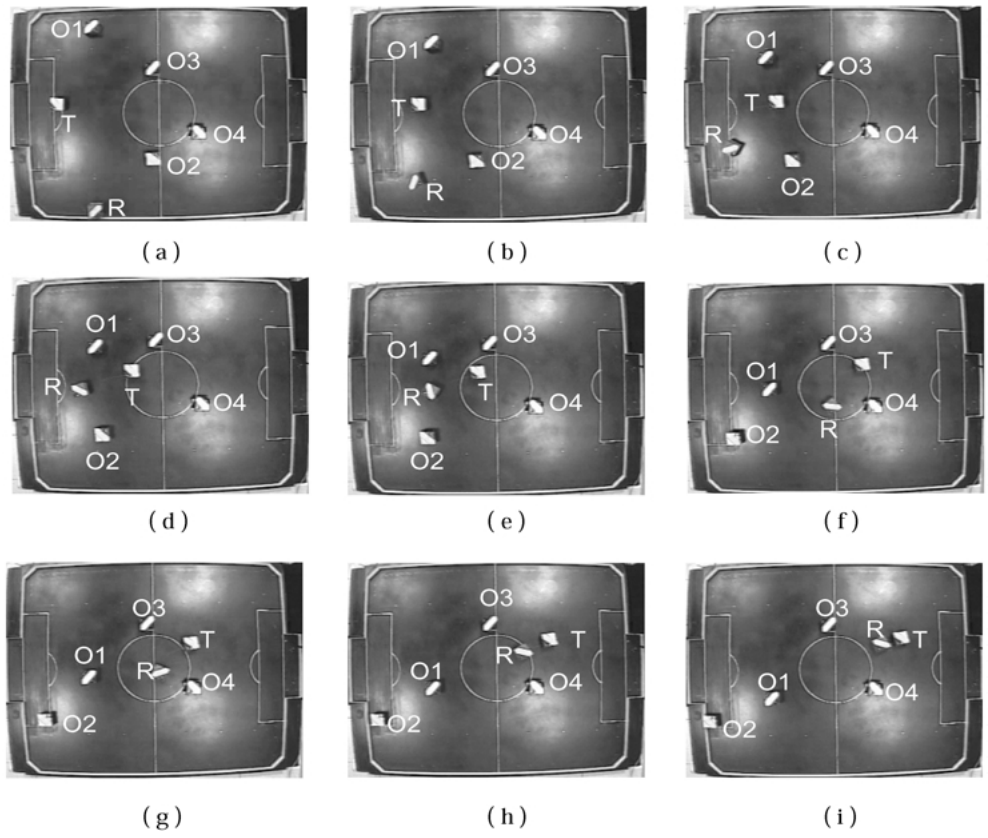

Figure 22. Experiment result with moving target and moving obstacles.

during the experiment, R being the robot under investigation, T the target robot which moved at constant velocity rightwards, O1 and O2 two moving obstacles with O1 moving downwards and O2 moving leftwards, O3 and O4 two stationary obstacles. Figure 22(a) shows the initial positions of each robot. As the robot R moved, it entered the influence range of the obstacle O2 and began to detour O2 from its front, as shown in Fig. 22(b). Figure 22(c) shows that the robot successfully detoured obstacle O2 and moved toward the target robot T again. As robot R moved on, it entered the influence range of obstacle O1, as shown in Fig. 22(d). Because the relative velocity of the robot toward O1 is positive, O1 generated repulsive force to push robot R away. As shown in Fig. 22(e), the robot R changed its moving direction and detoured O1 again from its front. Figure 22(f) shows that the robot successfully avoid the obstacle O1. From Figs. 22(g)–(i), it can be seen that the robot finally caught the target robot and at the same time avoid obstacles O3 and O4 successfully. The experiment has demonstrated that the proposed potential field method can be successfully used for mobile robot motion planning.

8. Conclusion

In this paper, a new potential field method has been proposed for mobile robot motion planning in a dynamic environment where both the target and obstacles are moving. The new potential functions take into account not only the relative positions of the robot with respect to the target and obstacles, but also the relative velocities of the robot with respect to the target and obstacles. Accordingly, the virtual force is defined as the negative gradient of the potential with respect to both position and velocity. The motion of the mobile robot is then determined by the total virtual force through the Newton's Law or steering control depending on the driving type of the robot. Computer simulations and hardware experiments have demonstrated the effectiveness of the mobile robot motion planning schemes based on the new potential field method.

References

Borenstein, J. and Koren, Y. 1989. Real-time obstacle avoidance for fast mobile robots. *IEEE Trans. Sys. Man, Cyb.*, 19(5):1179–1187.

Borenstein, J. and Koren. Y. 1991. The vector field histogram—fast obstacle avoidance for mobile robots. *IEEE Trans. Robotic. Autom.*, 7(3):278–288.

Canny, J.F. and Lin, M.C. 1990. An opportunistic global path planner. In *Proc. of IEEE Conf. Robotic. Autom.*, pp. 1554–1559.

Chuang, J.H. and Ahuja, N. 1998. An analytically tractable potential field model of free space and its application in obstacle avoidance. *IEEE Trans. Sys. Man, Cyb.—Part B: Cyb*, 28(5):729–736.

Conn, R.A. and Kam, M. 1998. Robot motion planning on N-dimensional star worlds among moving obstacles. *IEEE Trans. Robotic. Autom.*, 14(2):320–325.

Fujimura, K. and Samet, H. 1989. A hierarchical strategy for path planning among moving obstacles. *IEEE Trans. Robotic. Autom.*, 5(1):61–69.

Ge, S.S. and Cui, Y.J. 2000. New potential functions for mobile robot path planning. *IEEE Trans. Robotic. Autom.*, 16(5):615–620.

Guldner, J. and Utkin, V.I. 1995. Sliding mode control for gradient tracking and robot navigation using artificial potential fields. *IEEE Trans. Robot. Automat.*, 11:247–254.

Hussien, B. 1989. Robot path planning and obstacle avoidance by means of potential function method. Ph.D Dissertation, University of Missouri-Columbia.

Khatib, O. 1986. Real-time obstacle avoidance for manipulators and mobile robots. *Int. J. Robotics Research*, 5(1):90–98.

Khosla, P. and Volpe, R. 1988. Superquadric artificial potentials for obstacle avoidance and approach. In *Proc. IEEE Conf. Robotic. Autom.*, pp. 1778–1784.

Kim, J.O. and Khosla, P.K. 1992. Real-time obstacle avoidance using harmonic potential functions. *IEEE Trans. Robotic. Autom.*, 8(3):338–349.

Ko, N.Y. and Lee, B.H. 1996. Avoidability measure in moving obstacle avoidance problem and its use for robot motion planning. In *Proc. IEEE/RSJ Int. Conf. Intell. Robots and Sys.*, Vol. 3, pp. 1296–1303.

Kodtschek, D.E. 1989. The application of total engergy as Lyapunov function for mechanical control systems. In *Contemporary Mathematics*, Amer. Math. Soc.: Providence, RI, Vol. 97, pp. 131–157.

Latombe, J. 1991. *Robot Motion Planning*, Kluwer Academic Publishers: Boston.

Pin, F.G. and Killough, S.M. 1994. A new family of omnidirectional and holinomic wheeled platforms for mobile robots. *IEEE Trans. Robotic. Autom.*, 10(4):480–489.

Rimon, E. 1990. Exact robot navigation using artificial potential functions. Ph.D Dissertation, Yale University.

Rimon, E. and Koditschek, D.E. 1992. Exact robot navigation using artificial potential functions. *IEEE Trans. Robotic. Autom.*, 8(5):501–518.

Shih, C.L. and Lee, T. 1990. A unified approach for robot motion planning with moving polyhedral obstacles. *IEEE Trans. Sys. Man, Cyb.*, 20(4):903–915.

Veelaert, P. and Bogaerts, W. 1999. Ultrasonic potential field sensor for obstacle avoidance. *IEEE Trans. Robotic. Autom.*, 15(4):774–779.

Warren, C.W. 1989. Global path planning using artificial potential fields. In *Proc. IEEE Conf. Robotic. Autom.*, pp. 316–321.

Warren, C.W. 1990. Multiple robot path coordination using artificial potential fields. In *Proc. IEEE Conf. Robotic. Autom.*, pp. 500–505.

Watanabe, K. 1998. Control of an omnidirectional mobile robot. In *1998 2nd Int. Conf. Knowledge-Based Intell. Electro. Sys.*, pp. 51–60.

S.S. Ge received the B.Sc. degree from Beijing University of Aeronautics and Astronautics (BUAA), Beijing, China, in 1986, and the Ph.D. degree and the Diploma of Imperial College (DIC) from Imperial College of Science, Technology and Medicine, University of London, in 1993. From 1992 to 1993, he did his postdoctoral research at Leicester University, England. He has been with the Department of Electrical & Computer Engineering, the National University of Singapore since 1993, and is currently as an Associate Professor. He visited Laboratoire de'Automatique de Grenoble, France in 1996, the University of Melbourne, Australia in 1998, 1999, and University of Petroleum, Shanghai Jiaotong University, China, in 2001. He has authored and co-authored over 100 international journal and conference papers, two monographs and co-invented two patents. He served as an Associate Editor on the Conference Editorial Board of the IEEE Control Systems Society in 1998 and 1999, has been serving as an Associate Editor, IEEE Transactions on Control Systems Technology since 1999, and a member of the Technical Committee on Intelligent Control of the IEEE Control System Society since 2000. He was the winner of the 1999 National Technology Award, Singapore. He serves as a technical consultant local industry. He is currently a Senior Member of IEEE. His current research interests are Control of nonlinear systems, Neural Networks and Fuzzy Logic, Robot Control, Real-Time Implementation, Path Planning and Sensor Fusion.

Y.J. Cui received the B.E. and M.E. degrees from Northwestern Polytechnical University, China, in 1995 and 1997, respectively. During 1998–2001, she was a Research Scholar toward a Ph.D. degree in the Department of Electrical & Computer Engineering, National University of Singapore. In 2002, she joined Singapore Technologies Dynamics Pte Ltd. Her current research interests are Path Planning, Navigation, and Sensor Fusion.